PhD Thesis

Thesis Title

Jaime Travesedo Laso

October 20, 2025

The harmony of the world is made manifest in Form and Number, and the heart and soul and all the poetry of Natural Philosophy are embodied in the concept of mathematical beauty.

– D'Arcy Wentworth Thompson

Acknowledgements

Write your acknowledgements here.

Contents

List of Figures

List of Tables

1. Introduction

Introduction text here.

1.1. Motivation

Motivation text here.

1.2. Objectives

Objectives text here.

Background 2.

2.1. Erbium ions in Solids

Erbium belongs to the family of atoms known as lanthanides. These atoms have gathered significant interest as potential enablers for key quantum technologies such as quantum repeaters, memories and transducers. The unique properties of these atoms can be traced to their electronic structure. Their incomplete $4f$ valence shell is shielded by the outermost $5s$ and $5p$ closed shells from interacting with the environment, ligand electrons and lattice vibrations. This is particularly useful since these atoms can be placed in a crystalline host, where micro- and nanostructures can be fabricated to enhance their interaction with light, while maintaining long optical and spin coherences. In addition, Erbium has an optical transition at 1.5 µm, in the low-loss band of optical fiber, which can be exploited for integration in current network infrastructure.

This section will focus on the energy level structure of erbium when placed inside of a $CaWO_4$ host. Then, we will consider the interaction of the erbium ion with the nuclear spin environment of the crystal, mainly consisting of ^{183}W nuclear spins.

Free-ion Hamiltonian

Given the protection of the erbium energy states to external perturbations, we consider first the energy level structure of the free Er^{3+} ion, which is described in detail in the following references [1, 2]. To describe the energy of an ion we consider the following Hamiltonian.

[1]: Weissbluth (2012), *Atoms and Molecules*
[2]: Abragam et al. (2012), *Electron Paramagnetic Resonance of Transition Ions*

$$\begin{aligned}
\mathcal{H}_{FI} &= \mathcal{H}_0 + \mathcal{H}_C + \mathcal{H}_{SO}, \\
\mathcal{H}_0 &= -\sum_{i=1}^{N} \frac{\hbar^2}{2m}\nabla_i^2 - \sum_{i=1}^{N} \frac{Ze^2}{r_i}, \\
\mathcal{H}_C &= \sum_{i<j}^{N} \frac{e^2}{r_{ij}}, \\
\mathcal{H}_{SO} &= \sum_{i=1}^{N} \xi(r_i)\, \mathbf{l}_i \cdot \mathbf{s}_i.
\end{aligned} \tag{2.1}$$

Where r_i is the distance of each electron to the nucleus and r_{ij} are the distances between electrons. In order, the terms describe the kinetic and potential energy, the electron–electron Coulomb interaction and the spin–orbit coupling. For light ions, the spin–orbit coupling can be considered as a perturbation to the dominant electron–electron interaction. However, the Hamiltonian defined by the remaining terms cannot be directly solved, as it involves the coupling between N independent electrons. This problem is solved by introducing the central-field approximation, where the electron–electron interaction is described with a single-electron potential averaged over all electron interactions.

$$
\begin{aligned}
\mathcal{H}_{\mathrm{FI}} \approx & \mathcal{H}_{\mathrm{C}} + \mathcal{H}_{\mathrm{NC}} + \mathcal{H}_{\mathrm{SO}}, \\
\mathcal{H}_{\mathrm{C}} = & \sum_{i=1}^{N} \frac{\hbar^2}{2m} \nabla_i^2 - \sum_{i=1}^{N} \frac{Ze^2}{r_i} + \left\langle \sum_{\text{pairs}} \frac{e^2}{r_{ij}} \right\rangle \\
\mathcal{H}_{\mathrm{NC}} = & \sum_{\text{pairs}} \frac{e^2}{r_{ij}} - \left\langle \sum_{\text{pairs}} \frac{e^2}{r_{ij}} \right\rangle
\end{aligned}
\tag{2.2}
$$

From this expression, it is clear that $\mathcal{H}_{\mathrm{NC}}$ is merely a perturbation on $\mathcal{H}_{\mathrm{C}}$. This allows to separate $\mathcal{H}_0$ into N independent single-electron equations with the same angular properties as the Hydrogen atom. Each electron i will be described by the four quantum numbers (n, l, m_l, m_s), respectively the principal quantum number, the angular momentum quantum number $(0 \leq l < n-1)$, the magnetic quantum number $(-l \leq m_l \leq +l)$ and the spin quantum number $(m_s = \pm\frac{1}{2})$. For lanthanides, the valence shell is located in the $n = 4$ and $l = 3$ configuration and is generally refered as the $4f$ shell [1]. The averaged electron interaction term is not known, but it can be treated using the Hartree–Fock approximation (see [1]).

1: The actual electronic wavefunctions are given by a Slater determinant, which enforces the Pauli exclusion principle and the anti-symmetric behaviour under electron exchange that is characteristic of fermionic particles.

[1]: Weissbluth (2012), *Atoms and Molecules*

To calculate the effect of the non-central Hamiltonian $\mathcal{H}_{\mathrm{NC}}$, the matrix elements of the Hamiltonian are calculated in a shared diagonal basis. This basis exploits the fact that both the angular momentum operators $\mathbf{L}$ and the spin operators $\mathbf{S}$ commute with $\mathcal{H}_{\mathrm{FI}}$. This allows one to define a common basis with the set of eigenvectors of $\mathbf{L}^2$ and $\mathbf{S}^2$ (Russell–Saunders coupling).

Lastly, we consider the effects of the spin–orbit coupling on the energy structure. For light ions, with radially confined orbitals, this term is smaller than the rest of the interactions and can be treated as a perturbation. However, it is important to note that this term does not commute independently with $\mathbf{L}$ and $\mathbf{S}$ but with the combination of the two operators $\mathbf{J} = \mathbf{L} + \mathbf{S}$. Thus, the perturbation splits the degeneracy of the Russell–Saunders ground state into levels with a specific value of J, which are $(2J+1)$-degenerate. The labels are given by Russell–Saunders notation as ${}^{2S+1}L_J$[2]. In the case of Er^{3+} , the free-ion ground state corresponds to ${}^4I_{15/2}$, a 16-fold degenerate level. The first excidecited level is separated by 1.5 µm. In the following work, the $CaWO_4$ crystal and the ions are cooled down to 10 mK. Consequently, only the ground state will be populated, which can be effectively approximated as a spin $J = 15/2$.

2: Since erbium is a medium-sized ion, this approximation is not entirely valid, given that the spin–orbit coupling is no longer perturbative. Thus, J and S are no longer good quantum numbers, but remain relatively accurate for low-energy transitions.

Crystal-field Hamiltonian

When a lanthanide enters a crystal, it does so as a trivalent ion. Inside the crystal, the ion will be subject to the electrostatic field generated by the electronic clouds of the neighboring atoms. The crystal field breaks the spherical symmetry, which lifts the degeneracy of the free-ion states. However, the $4f$ electrons of a lanthanide are highly localized and shielded, so the crystal-field interaction can be treated as a perturbation to the free-ion energy levels.

We begin the section with a description of the host crystal. Calcium tungstate ($CaWO_4$), also known as scheelite, is a tetragonal crystal appearing as dipyramidal pseudo-octahedra and belongs to the $I4_1/a$ symmetry group. The crystal structure of $CaWO_4$ consists of Ca^{2+} and W^{6+} ions coordinated by O^{2-} ions. Each Ca^{2+} ion is surrounded by eight O^{2-} ions, forming a distorted dodecahedral environment, while each W^{6+}

ion is tetrahedrally coordinated by four O^{2-} ions. The arrangement of these polyhedra leads to orthogonal principal axis (labeled as a, b and c). Due to the symmetry of the crystal the a- and b- axis are equivalent. The unit cell parameters at cryogenic temperature are $a = b = 5.23643$ Å and $c = 11.3381$ Å [3].

[3]: Senyshyn et al. (2004), 'Lattice Dynamics and Thermal Properties of CaWO4'

Lanthanide ions enter the crystal in substitution to Ca^{2+}. Due to the difference in charge between the two ions, charge compensation mechanisms take place inside the crystal, which can be achieved by the presence of interstitial ions, vacancies, or other defects. Figure (figure) shows an example of a $CaWO_4$ crystal, where an Er^{3+} replaces the central calcium ion. The point symmetry of the Er^{3+} site is S_4, which notably lacks inversion symmetry. (discussed later).

The crystal-field Hamiltonian is used to describe the interaction between the ion and the crystal and is generally described in terms of the extended Stevens operators $\hat{O}_k^q$ with $k = 2, 4, 6, \ldots$ and $q \in \{-k, \ldots, k\}$ [2, 4]

[2]: Abragam et al. (2012), *Electron Paramagnetic Resonance of Transition Ions*
[4]: Stevens (1952), 'Matrix Elements and Operator Equivalents Connected with the Magnetic Properties of Rare Earth Ions'

$$\mathcal{H}_{\mathrm{CF}} = \sum_{k}^{2,4,6,\ldots} \sum_{q}^{-k,\ldots k} B_k^q \hat{O}_k^q \tag{2.3}$$

Where B_k^q are the real-valued crystal field parameters. The extended Stevens operators are constructed as polynomial combinations of the J_z, J_+ and J_- operators, and a full list of the operators can be found in [7]. The indices k and q encode the symmetry properties of the crystal field: k specifies the rank of the operator (i.e., the maximum total power of angular momentum operators in the polynomial), and is restricted to even values due to time-reversal symmetry. The index q determines the projection to the quantization axis (i.e. the maximum power of the non-diagonal terms). This allows the crystal field to encode the symmetry properties of the crystal site in a reduced number of terms. The values of the crystal-field parameters for Er^{3+} :$CaWO_4$ are given in table 2.1.

B_2^0	231 cm^{-1}
B_4^0	-90 cm^{-1}
B_4^4	852 cm^{-1}
B_6^0	-0.6 cm^{-1}
B_6^4	396 cm^{-1}
B_6^{-4}	75 cm^{-1}

Table 2.1.: Crystal field parameters for Er^{3+} :$CaWO_4$ measured in [5] with the operator normalization as defined in [6]

The effect of the crystal-field is the mixing of states with different J and J_z, although the former is much weaker. For Er^{3+} , the 16-fold degenerate $^4I_{15/2}$ ground state is split into eight doublets ($Z_{1,\ldots,8}$), known as *Kramers doublets*. According to Kramers' theorem, [8] if the number of electrons in the $4f$ shell is odd and there is time-reversal symmetry (i.e. no magnetic field applied), then all crystal field levels are at least doubly degenerate, which is the case for Er^{3+} with $N = 11$.

[7]: Al'tshuler et al. (1964), *Electron Paramagnetic Resonance*

[8]: Kramers (1930), 'General Theory of Paramagnetic Rotation in Crystals'

Each of the doublets can be modelled as an effective spin-1/2 with an anisotropic gyromagnetic factor that depends on the mixing between the J_z wavefunctions. The energy difference between the Z_1 and Z_2 doublets is approximately 0.6 THz, which corresponds to a temperature of 50 K. At cryogenic temperatures (generally between 10 mK and 100 mK), only the Z_1 doublet will be populated, and the system can be effectively treated as an effective spin-1/2. During much of this work, this approximation will be used. Nevertheless, it is important to note that the application of a magnetic field can further mix the J-multiplet states, modifying the effective spin properties.

Under a magnetic field $\mathbf{B_0}$, the Hamiltonian of the ground $J = 15/2$-multiplet can be written as

$$\mathcal{H}_J = \mu_B \, g_J \mathbf{B_0} \cdot \mathbf{J} + \mathcal{H}_{\mathrm{CF}}, \tag{2.4}$$

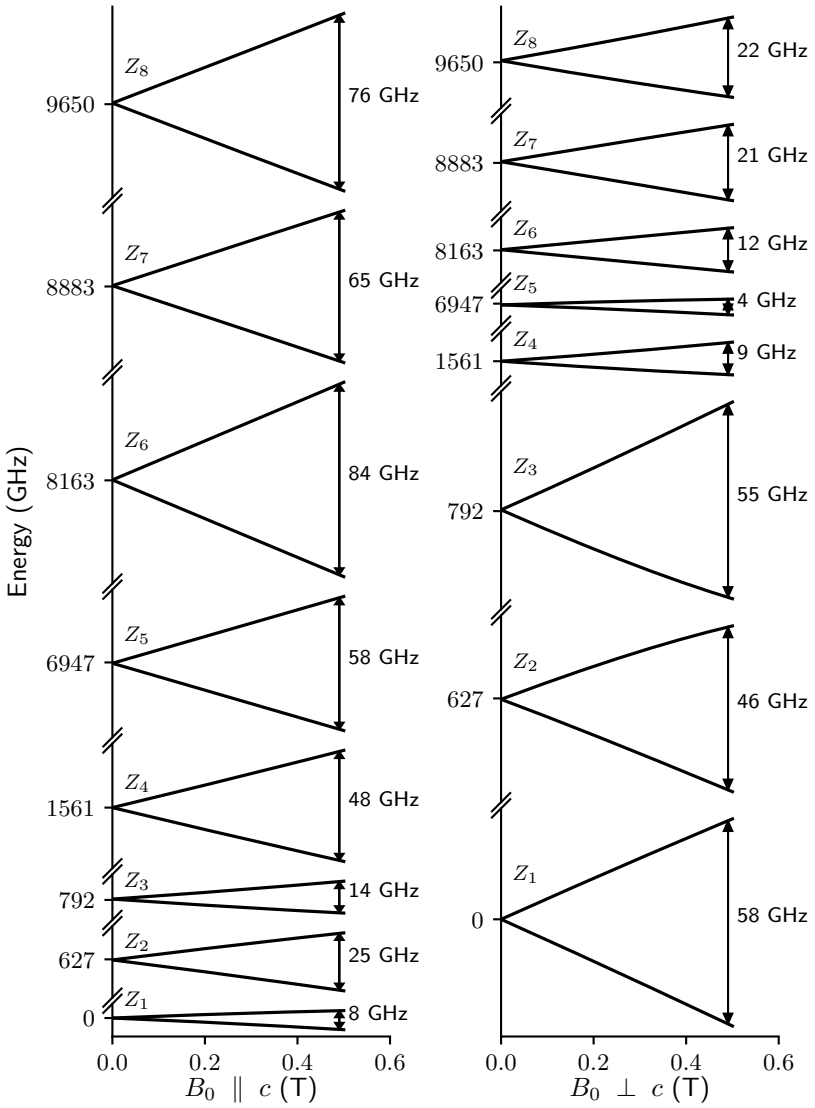

Figure 2.1.: Energy levels for all Z_i doublets under a magnetic field parallel (perpendicular) to the *c*-axis. The y-axis is broken to better show the magnetic splitting of the levels. Energy difference between the states of each doublet at 500 mT is shown as vertical double arrows, along with the approximate frequency of the transitiion

The first term represents the Zeeman interaction, where $\mu_B/2\pi = 13.996$ GHz/T is the Bohr magneton and $g_J = 6/5$ is the Landé factor for the Er^{3+} ground state. Figure 2.1 illustrates the magnetic-field-induced splitting of the energy levels along the *c*-axis, obtained by direct diagonalization of the Hamiltonian in Eq. 2.4. Each Z_i doublet splits into two levels, with an effective, anisotropic gyromagnetic tensor that varies for each doublet. This anisotropy is evident from the differing transition frequencies observed when a 500 mT magnetic field is applied parallel versus perpendicular to the *c*-axis.

Spin-1/2 approximation

The energy separation between the Z_1 and Z_2 doublets is approximately 650 GHz, which corresponds to a temperature of 50 K. Thus, at the working temperature of 10 mK, only the Z_1 doublet will be populated. This doublet can be effectively treated as a spin-1/2 with an anisotropic gyromagnetic tensor,

$$\mathcal{H}_S = \mathbf{B_0} \cdot \bar{\bar{\gamma}}_{^{3+}\mathrm{Er}} \cdot \mathbf{S} \tag{2.5}$$

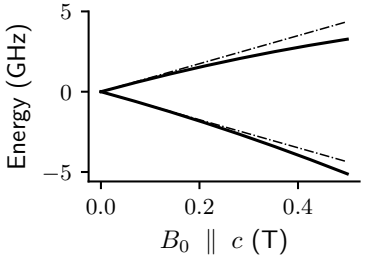

Figure 2.2.: Energy levels of the Z_1 doublet as a function of magnetic field along the *c*-axis. The curves were obtaioned by direct diagonalization of Eq. 2.4 and Eq. 2.5 (solid and dot-dashed resp.).

with two eigenstates $|\downarrow\rangle$ and $|\uparrow\rangle$. The effective gyromagnetic tensor $\bar{\bar{\gamma}}_{^{3+}\mathrm{Er}}$ is diagonal along the principal axes of the crystal, with values [9]

[9]: Antipin, A.A. et al. (1981), 'Anisotropy of Er3+ Spin-Lattice Relaxation in LiYF4 Crystals'

$$\begin{aligned} \gamma_a = \gamma_b = \gamma_\perp &= -2\pi \times 117.3\ \mathrm{GHz/T}, \\ \gamma_c = \gamma_\parallel &= -2\pi \times 17.45\ \mathrm{GHz/T}. \end{aligned} \tag{2.6}$$

Throughout this thesis, we will primarily use this effective spin-1/2 approximation for the energy structure of the Er^{3+} . Nevertheless, it is important to note that as the magnetic field increases, mixing between doublets becomes significant, leading to deviations from the simple linear Zeeman splitting. This effect is illustrated in Figure 2.2, where the energy levels of the Z_1 doublet are shown alongside the linear approximation as a function of magnetic field along the c-axis. Compared to the linear behaviour of the spin-1/2 approximation, the energy levels obtained from the crystal-field Hamiltonian "bend" as the magnetic field increases. A direct result of this non-linear behaviour is the appearance of a non-zero average magnetic moment

$$\langle \mu_z \rangle = \frac{\partial E_\downarrow}{\partial B_0} - \frac{\partial E_\uparrow}{\partial B_0} \neq 0 \tag{2.7}$$

where $E_\downarrow$ and $E_\uparrow$ are the energies of the system as a function of the applied magnetic field B_z. This non-linearity is the origin of the pseudo-Zeeman [10] and pseudo-Quadrupole effects [11], which are taken into account when interpreting the high-resolution spectroscopy experiments detailed in (labch)

[10]: Baker et al. (1997), 'Paramagnetic Resonance in Some Lanthanon Ethyl Sulphates'

[11]: Foley (1947), 'Second-Order Magnetic Perturbations in Nuclear Quadrupole Spectra and the "Pseudo-Quadrupole" Effect in Diatomic Molecules'

Magneto-Electric effect

As discussed before, Er^{3+} :$CaWO_4$ is located in a site with S_4 symmetry, which notably lacks inversion symmetry. This results in the appearance of odd terms ($k = 1, 3, 5, \dots$) in the crystal-field Hamiltonian. However, these terms do not modify the energy level structure of the ion unless an external electric field is applied [12]. The origin of these magneto-electric shifts lies in the electrical-field-induced mixing between the odd and even terms of the Hamiltonian [13]. This interaction can be modeled with the following Hamiltonian,

[12]: Ham (1961), 'Linear Effect of Applied Electric Field in Electron Spin Resonance'

[13]: Kiel et al. (1970), 'Electric-Field-Induced g Shifts for Loose Yb Ions in Three Scheelite Lattices'

$$\mathcal{H}_{\text{m-e}} = \sum_{i,j,k}^{\{a,b,c\}} T_{k,i,j} S_i B_j E_k \tag{2.8}$$

where $i, j, k \in \{x, y, z\}$ and $T_{k,i,j}$ is third-rank tensor which is symmetric in the i, j indices. The tensor captures the linear mixing of the levels as a function of the electric and magnetic field. The values for the tensor in Er^{3+} :$CaWO_4$ were experimentally determined by Mims [14] and are displayed in Table 2.2. The effect can be described with only four independent parameters and the rest of the elements of the tensor are obtained by enforcing S_4 and $\{i, j\}$ index symmetry.

param.	value	S_4 symm.
$T_{a,c,a}$	1.4	$-T_{b,c,b}$
$T_{a,c,b}$	1.0	$-T_{b,c,a}$
$T_{c,a,a}$	5.4	$-T_{c,b,b}$
$T_{c,b,a}$	2.9	(-)

Table 2.2.: Magneto-electric parameters for Er^{3+} :$CaWO_4$ given in ($10^{-32} \times \frac{\mathrm{J/T}}{\mathrm{V/m}}$). The third column indicates the relation between the parameters that originate from the S_4 symmetry of the ion site. The rest of the values of the tensor can be obtained by enforcing $\{i, j\}$ index symmetry $T_{k,i,j} = T_{k,j,i}$.

(Plot with the shift as a function of the electric field)

Even if the energy shifts are zero in the absence of and electric field, this interaction can be understood as an induced electric dipole $\mathbf{d}$ due to an

[14]: Mims (1965), 'Electric Field Shift in Paramagnetic Resonance for Four Ions in a Calcium Tungstate Lattice'

external magnetic field; if **B** is fixed, the interaction can be effectively rewritten as

$$\begin{aligned} \mathcal{H}_{\text{m-e}} &= \sum_k -d_k E_k = -\mathbf{d}\cdot\mathbf{E}, \\ d_k &= -\sum_{i,j} T_{k,i,j}\langle S_i\rangle B_j. \end{aligned} \tag{2.9}$$

where $\langle S_i\rangle$ corresponds to the expected value of the electron spin. The dipole in turn generates an electric field around the position of the Er^{3+}, whose effects will be revisited in (refsec)

Magnetic spin environment

The nuclear spin environment of $CaWO_4$ is predominantly composed of ^{183}W nuclear spins, which have a natural abundance of 14.4% and a relatively low gyromagnetic ratio, $\gamma_{^{183}W}/2\pi = 1.77394$ MHz/T [15]. The combination of a low density of nuclear spins and a weak gyromagnetic ratio results in an environment with a reduced magnetic moment density. [3] As such, the magnetic noise perceived by any paramagnetic impurity hosted in the crystal is significantly reduced compared to other hosts used in quantum applications, such as yttrium orthosilicate (Y_2SiO_5, YSO) and yttrium oxide (Y_2O_3). This results in slow spectral diffusion and reduced decoherence rates for any paramagnetic impurity hosted in the crystal.

In addition to the nuclear spin bath, paramagnetic impurities—such as other rare-earth ions or transition metal ions—can also contribute significantly to the magnetic environment experienced by a single Er^{3+} ion. These electronic spins have a much larger gyromagnetic response and are more spatially delocalized than the point-like nuclear spins. At high concentrations, the magnetic noise is dominated by the paramagnetic impurities rather than the nuclear bath. Therefore, minimizing the dopant concentration is crucial to achieve long coherence times. Indeed, by reducing the concentration of rare-earth ions to the 1–100 parts per billion (ppb) range and exploiting the low magnetic density, ensemble spin coherence times as long as 23 ms have been demonstrated for Er^{3+}:$CaWO_4$ [16].

The sample used for this work was grown using high-purity, natural-abundance materials and no paramagnetic impurities were added during crystal growth[4]. Nevertheless, trace amounts in the precursors result in a concentration of Er^{3+} of 3.1 ppb, measured using electron spin resonance (ESR) techniques (appendix). There are four calcium sites in a single unit cell with volume $V_{\text{unit cell}} \sim 310$ Å^3. This results in in average distance between ions of 0.3 µm. [5] This distance is large enough that interactions between paramagnetic impurities can be effectively neglected except in specific cases where two ions are, by chance, in close proximity. Consequently, we consider that the magnetic environment in the crystal is dominated by ^{183}W nuclear spin.

Interaction between two spins

We now consider interactions between two spins, which in this system are governed primarily by two mechanisms: long-range magnetic dipole cou-

[15]: Knight et al. (1986), 'Solid-State Tungsten-183 Nuclear Magnetic Resonance Spectroscopy'

3: There are other stable calcium and oxygen isotopes with non-zero nuclear spin, namely ^{43}Ca, ^{15}O and ^{17}O with $I = 7/2$, $I = 1/2$ and $I = 5/2$, respectively, but their natural abundances are low (0.1%, 0.003% and <0.003%, respectively) and are not considered in our discussion.

[16]: Le Dantec et al. (2021), 'Twenty-Three–Millisecond Electron Spin Coherence of Erbium Ions in a Natural-Abundance Crystal'

4: Specific details on the growth of a similar sample can be found in [17].

5: The Ca site density is

$$4/310 \approx 1.3\times10^{-2}\ \text{A}^{-3}$$

With $[Er^{3+}]$=3.1 ppb, the Er^{3+} density is

$$n_{Er^{3+}} \approx 4.0\times10^{-11}\ \text{A}^{-3}$$

and the characteristic spacing is

$$n_{Er^{3+}}^{-1/3} \approx 2.9\times10^{3}\ \text{A} \approx 0.29\ \mu\text{m}$$

pling and short-range contact interaction. Below we treat Er^{3+} -^{183}W and ^{183}W -^{183}W couplings separately. Due to the very low Er^{3+} concentration, Er^{3+} -Er^{3+} interactions are negligible and are therefore omitted.[6]

6: A complete analysis of Er^{3+} decoherence should include interactions between paramagnetic ions, but this lies outside the scope of the present work.

Magnetic dipole interaction

In classical physics, the magnetic interaction between two dipoles with magnetic vector moments $\boldsymbol{\mu_1}$ and $\boldsymbol{\mu_2}$ is expressed as[2]

[2]: Abragam et al. (2012), *Electron Paramagnetic Resonance of Transition Ions*

$$\mathcal{H}_{dd} = \frac{\mu_0}{4\pi} r^{-3} \left[\boldsymbol{\mu}_1 \cdot \boldsymbol{\mu}_2 - 3r^{-2} (\boldsymbol{\mu}_1 \cdot \mathbf{r})(\boldsymbol{\mu}_2 \cdot \mathbf{r}), \right] \tag{2.10}$$

where $\mathbf{r}$ is the vector separating the two dipoles. In quantum mechanics, this expression is directly applicable when taking into consideration that the magnetic moment of a spin is given by $\boldsymbol{\mu} = \bar{\bar{\gamma}} \cdot \mathbf{S}$. Expanding the expression in terms of the spin operators yields

$$\begin{aligned}
\mathcal{H}_{dd} = \frac{\mu_0}{4\pi} r^{-3} \Big[& \gamma_{x1}\gamma_{x2}\hat{S}_{x1}\hat{S}_{x2}\left(1 - 3\sin^2\theta_r \cos^2\phi_r\right) \\
& + \gamma_{y1}\gamma_{y2}\hat{S}_{y1}\hat{S}_{y2}\left(1 - 3\sin^2\theta_r \sin^2\phi_r\right) \\
& + \gamma_{z1}\gamma_{z2}\hat{S}_{z1}\hat{S}_{z2}\left(1 - 3\cos^2\theta_r\right) \\
& - 3\sin^2\theta_r \cos\phi_r \sin\phi_r \left(\gamma_{x1}\gamma_{y2}\hat{S}_{x1}\hat{S}_{y2} + \gamma_{y1}\gamma_{x2}\hat{S}_{y1}\hat{S}_{x2}\right) \\
& - 3\sin\theta_r \cos\phi_r \cos\theta_r \left(\gamma_{x1}\gamma_{z2}\hat{S}_{x1}\hat{S}_{z2} + \gamma_{z1}\gamma_{x2}\hat{S}_{z1}\hat{S}_{x2}\right) \\
& - 3\sin\theta_r \sin\phi_r \cos\theta_r \left(\gamma_{y1}\gamma_{z2}\hat{S}_{y1}\hat{S}_{z2} + \gamma_{z1}\gamma_{y2}\hat{S}_{z1}\hat{S}_{y2}\right) \Big]
\end{aligned} \tag{2.11}$$

where θ_r and ϕ_r are respectively the polar and azimutal angles of the $\mathbf{r}$ vector. This interaction can be expressed following compact form

$$\mathcal{H}_{\text{d-d}} = \mathbf{S_1} \cdot \bar{\bar{A}} \cdot \mathbf{S_2}, \tag{2.12}$$

where the complexity of the dipolar interaction is encoded in the hyperfine tensor $\bar{\bar{A}}$. This interaction is strongly anisotropic and depends on the relative position and orientation between the two spins. Therefore, their coupling will depend on the orientation of the external magnetic field. This is particularly relevant in the case of Er^{3+} :$CaWO_4$ as the erbium spin is strongly anisotropic.

We first consider the interaction between the Er^{3+} electron spin and the ^{183}W nuclear spin ($\mathbf{S_1} = \mathbf{S}$ and $\mathbf{S_2} = \mathbf{I}$). The particularity of this case arises from the large difference between the Zeeman energies of the two spins: the gyromagnetic tensor of electrons is approximately 10^3 times larger than that of nuclear spins. In addition, we consider the large-field regime[7], where the dominant term in the Hamiltonian is the Zeeman energy of Er^{3+} . In line with the experimental conditions discussed later, we take the magnetic field to be approximately parallel to the c-axis of the crystal, corresponding to the z-axis of the laboratory frame. The leading contribution to the Hamiltonian is then S_z, while non-commuting terms can be treated as perturbations to the energy-level structure. In particular, hyperfine interaction terms involving S_x and S_y can be disregarded by applying the secular approximation. The resulting Hamiltonian is given by

7: This corresponds to

$$|\bar{\bar{\gamma}}_{^3+\text{Er}} \cdot \mathbf{B_0}| \gg \bar{\bar{A}}.$$

If the separation between the spins is a, the condition can be approximated as

$$|\mathbf{B_0}| \gg \frac{\gamma_{^{183}\text{W}}\mu_0}{8\pi a^3} \approx 1\ \text{mT}.$$

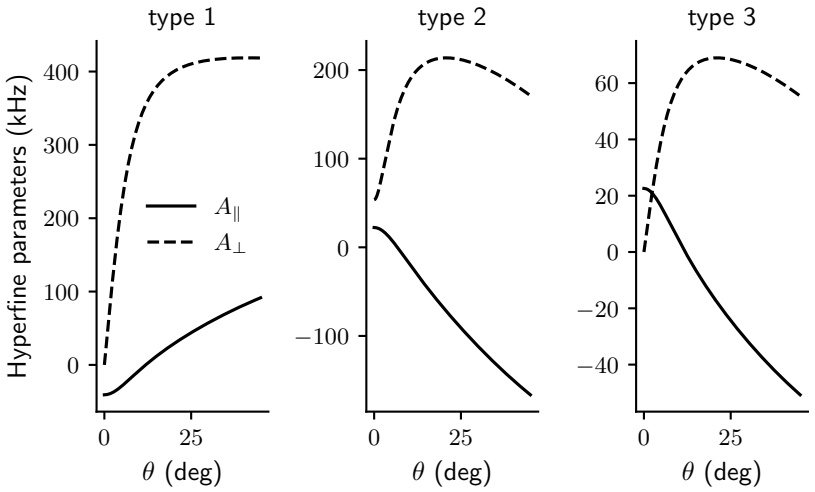

Figure 2.3.: Parallel and perpendicular hyperfine couplings as a function of the angle θ between the magnetic field B_0 and the c-axis of the crystal for the three types of W-sites.

$$\begin{aligned}\mathbf{S}\cdot\bar{\bar{A}}\cdot\mathbf{I} \approx S_z\ \left(A_{zx}I_x + A_{zy}I_y + A_{zz}I_z\right) \rightarrow \\ \rightarrow S_z\ \left(A_\perp I_x + A_\parallel I_z\right),\end{aligned} \tag{2.13}$$

where the arrow corresponds to a rotation of the coordinate system by x-axis lies along the direction of the perpendicular hyperfine coupling and $A_\perp^2 = A_{zx}^2 + A_{zy}^2$ and $A_\parallel = A_{zz}$.

Intuitively, the secular approximation can be understood by considering the effects of each term in the Er^{3+} spin Bloch sphere. The dominant Zeeman term induces a precession of the electron spin around the z-axis with frequency $\gamma_\parallel B_0$. By contrast, the hyperfine terms involving S_x and S_y correspond to rotations around the x- and y-axes, with much smaller frequencies. Because of the large difference in frequency scales, the transverse rotations effectively average to zero and can be neglected.

Within the first unit cell, and with B_0 applied parallel to the c-axis, three sets of magnetically-equivalent ^{183}W atoms can be found, called types 1, 2, and 3 in the following. All ^{183}W nuclear spins beyond the first unit cell have lower couplings and are not resolved in this work. Table Table 2.3 indicates the atomic positions of the ten W-sites within a unit cell centered around an Er^{3+} ion. The value of the hyperfine parameters $A_\parallel$ and $A_\perp$ are plot as a function of the angle between the applied magnetic field and the c-axis is Figure 2.3. The strong dependence of the hyperfine coupling with the angle evidences the anisotropic nature of the interaction, with values that can change from a zero to hundreds of kHz in less than 10º.

	distance (Å)
type 1	(+2.62, +2.62, 0)
	(+2.62, −2.62, 0)
	(−2.62, +2.62, 0)
	(−2.62, −2.62, 0)
type 2	(+2.62, 0, −2.84)
	(−2.62, 0, −2.84)
	(0, +2.62, +2.84)
	(0, −2.62, +2.84)
type 3	(0, 0, +5.69)
	(0, 0, −5.69)

Table 2.3.: W site positions in $CaWO_4$, separated in three types depending on their relative position to the central Er^{3+} ion

For the case between two ^{183}W nuclear spins (with spin operators $\mathbf{I_1}$ and $\mathbf{I_2}$), we give a rough estimation of the interaction strength as a full picture of the coupling between the different sites will is not of interest in this work. Since both spins are have an isotropic gyromagnetic factor, they will both be aligned to the externally applied field in the high field regime. For two aligned spins the interaction is then simplified to

$$\mathcal{H}_{\text{d-d}} = \frac{\mu_0\gamma_{^{183}\text{W}}^2}{4\pi r^3}\mathbf{I_1}\mathbf{I_2}\left[1 - 3\cos(\theta_r)\right], \tag{2.14}$$

and the average strength of the interaction is

$$\frac{\mu_0 \gamma_{^{183}\mathrm{W}}^2}{8\pi a^3} \approx 1 \text{ Hz}, \tag{2.15}$$

is orders of magnitude smaller than the Er^{3+} -^{183}W coupling and Zeeman terms. Therefore, the nuclear spin bath interactions will be slow compared to the dynamics of the paramagnetic ion and the neighbouring nuclear spins.

Exchange interaction

The exchange interaction, also known as Fermi-contact interaction, takes the following form [2]:

[2]: Abragam et al. (2012), *Electron Paramagnetic Resonance of Transition Ions*

$$\mathcal{H}_{\text{exch}} = \mathbf{S_1} \cdot \bar{\bar{J}}_{\text{exch}} \cdot \mathbf{S_2} \tag{2.16}$$

Contact interactions only occur when the spin wavefunctions overlap with each other and the typical interaction range is ~1.5 nm [18]. We do not consider contact interactions between two nuclear spins as the wavefunctions are almost point-like.

[18]: Schweiger et al. (2001), *Principles of Pulse Electron Paramagnetic Resonance*

The wavefunctions of Er^{3+} ions are highly localized thanks to the $5s$ and $5p$ shielding. Additionally, thanks to the low density of Er^{3+} ions we can discard any possible contact term between two distant electron spins.

In the case of electron and nuclear spin interaction, the Er^{3+} and W ions in the crystal are coordinated by an oxygen ion (see (labfig)) which prevents direct overlap between the spin wavefunctions. We conclude that contact interaction between proximal Er^{3+} ions and ^{183}W nuclear spins is not the primary coupling; at most they may produce small isotropic shifts.

We conclude that the dominating interaction mechanism between two spins in our system is the free-space dipolar coupling.

Electric Quadrupole interaction

In section (labsec) we discuss the measurements performed in a system consisting of an Er^{3+} spin and a ^{93}Nb nuclear spin in close proximity. Although unexpected, the presence of a ^{93}Nb spin gave us the chance to study a more complex system, as it boasts a high nuclear spin $I = 9/2$. This requires introducing the nuclear quadrupole interaction[8], which couples the nuclear electric quadrupole moment to the local electric-field gradient (EFG)

8: The quadrupole is strictly zero for $I = \frac{1}{2}$

Physically, the quadrupole effect arrises from the non-sphericity of the nuclear wavefunctions of $I \geq 1$ nuclear spins. The charge distribution inside of the nuclear spin will be elongated and when subject to an external field gradient certain orientations of the charge will be favoured. Figure 2.4 sketches this intuition by placing an elongated positively charged distribution between four charges, two $+q$ in the x-axis and two $-q$ in the y-axis. Due to the electrostatic attraction between the positive and negative charges, the vertical orientation will be energetically favoured.

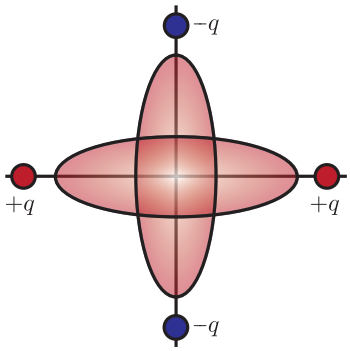

Figure 2.4.: Non-spherical charge distribution with four charges, two $+q$ in the x-axis and two $-q$ in the y-axis. The positively charged distribution has two orientations: perpendicular and horizonatal. The perpendicular orientation is energetically more favourable.

We now proceed to sketch the derivation of the quadrupole interaction in terms of the spin operators which can be found in full in [19]. We begin by considering the classical case of a charge distribution $\rho(\mathbf{r})$ under an electric potential $V(\mathbf{r})$. The energy associated to this system is given by

[19]: Slichter (1996), *Principles of Magnetic Resonance*

$$E = \int \rho(\mathbf{r}) \times V(\mathbf{r}) d\mathcal{V}. \tag{2.17}$$

We can approach this problem through the multi-pole expansion, which consists on writing the potential as a Taylor series at the center of mass of the nucleus and treating each term independently,

$$V(\mathbf{r}) = V(0) + \sum_{\alpha} x_\alpha \left.\frac{\partial V}{\partial x_\alpha}\right|_{\mathbf{r}=0} + \frac{1}{2!} \sum_{\alpha,\beta} x_\alpha x_\beta \left.\frac{\partial^2 V}{\partial x_\alpha \partial x_\beta}\right|_{\mathbf{r}=0} + \cdots \tag{2.18}$$

Consequently, the energy will be written as [9]

$$\begin{aligned} E = V(0) \int \rho \, d\mathcal{V} + \sum_{\alpha} V_\alpha \int x_\alpha \rho \, d\mathcal{V} + \\ + \frac{1}{2!} \sum_{\alpha,\beta} V_{\alpha\beta} \int x_\alpha x_\beta \rho \, d\mathcal{V} + \cdots \end{aligned} \tag{2.19}$$

9: We have introduced the notation

$$V_\alpha = \frac{\partial V}{\partial x_\alpha}, \quad V_{\alpha\beta} \equiv \frac{\partial^2 V}{\partial x_\alpha \partial x_\beta},$$

which correspond to the electric field and the EFG respectively.

Respectively, each term corresponds to the electrostatic energy of a point-charge nucleus, the energy due to the dipole moment [10] and the quadrupolar term. To describe the quadrupole interaction, it is particularly useful to introduce the following quantities

10: Given that the center of mass and the center of charge are equal, the dipole energy tends to zero

$$Q_{\alpha\beta} = \int \left(3x_\alpha x_\beta - \delta_{\alpha\beta} r^2\right) \rho \, d\mathcal{V} \tag{2.20}$$

as the energy of the quadrupole can be written in a compact form

$$E_{\mathrm{Q}} = \tfrac{1}{6} \sum_{\alpha,\beta} Q_{\alpha\beta} V_{\alpha\beta}. \tag{2.21}$$

To quantize this expression one must take the quantum mechanical expression for the charge density of the constituting protons of the nucleus and apply the Wigner-Eckart theorem to evaluate the resulting integrals and express the interaction in terms of the nuclear spin operator $\mathbf{I}$

$$\mathscr{H}_{\mathrm{Q}} = \frac{e\mathbb{Q}}{6I(2I-1)} \sum_{\alpha,\beta} V_{\alpha\beta} \left[\tfrac{3}{2}\left(I_\alpha I_\beta + I_\beta I_\alpha\right) - \delta_{\alpha\beta} I^2\right]. \tag{2.22}$$

where $\mathbb{Q}$ denotes the quadrupole moment, obtained from the integral of the nuclear charge distribution and measured in Barns. The quadrupole Hamiltonian can be writen the following compact form

$$\mathscr{H}_{\mathrm{Q}} = \mathbf{I} \cdot \bar{\bar{Q}} \cdot \mathbf{I}, \tag{2.23}$$

where $\bar{\bar{Q}}$ is the quadrupole tensor, proportional to the EFG. The EFG satisfies Laplace's equation, so its components obey $V_{xx} + V_{yy} + V_{zz} = 0$, and by electrostatic symmetry $V_{\alpha\beta} = V_{\beta\alpha}$. Consequently, the EFG (and thus $\bar{\bar{Q}}$) is a real, symmetric, traceless rank-2 tensor and can be diagonalized. In the principal-axis frame $(\mathbf{x}_Q, \mathbf{y}_Q, \mathbf{z}_Q)$, choosing the $\mathbf{z}_Q$

axis so that $|V_{z_Q z_Q}| \geq |V_{x_Q x_Q}| \geq |V_{y_Q y_Q}|$, one defines the conventional asymmetry parameter

$$\eta = \frac{V_{x_Q x_Q} - V_{y_Q y_Q}}{V_{z_Q z_Q}}, \qquad 0 \leq \eta \leq 1, \tag{2.24}$$

and the Hamiltonian in the principal-axis system can be expressed as

$$\mathscr{H}_Q = \frac{\hbar\omega_Q}{6}\left[3I_{z_Q}^2 - I(I+1) + \eta(I_{x_Q}^2 - I_{y_Q}^2)\right], \tag{2.25}$$

where $\hbar\omega_Q$ is the quadrupole energy[11]. Based on the value of the asymmetry parameter we can distinguish two regimes. First, if $\eta = 0$ the quadrupole is said to be axial and the Hamiltonian is diagonal in the $|I, m_I\rangle$ basis. The quadrupole then splits the nuclear energy levels by $m_I^2\omega_Q/2$, where m_I is the projection of the nuclear spin along the z_Q axis. Second, when $\eta \neq 0$ the term proportional to η mixes states differing by $\Delta m_I = \pm 2$ and creates a non-trivial energy level structure.

11: $$\omega_Q \equiv \frac{3e\mathbb{Q}V_{z_Q z_Q}}{2I(2I-1)\hbar}$$

Rotational invariance of the Quadrupole Hamiltonian

(In this section we now consider the reconstruction procedure of a quadrupole tensor of a spin under a magnetic field and the inherent limitations with only one magnetic field orientation.)

When measuring the nuclear spin transitions under a specific magnetic field orientation, the resulting frequencies are generally not enough to describe the full quadrupole tensor.

To unveil any hidden symmetry, it is useful to express the quadrupole in the basis of the rank-2 spherical tensors[12]. By algebraic manipulation of Eq. 2.22 we can rewrite the Hamiltonian as

$$\mathscr{H}_Q = \sum_{m=-2}^{2} Q_m T_m^{(2)}(\mathbf{I}) \tag{2.26}$$

12: The rank-2 spherical tensors are related to the spin operator basis by

$$T_0^{(2)} = 3I_z^2 - I(I+1),$$
$$T_{\pm1}^{(2)} = \mp(I_z I_\pm + I_\pm I_z),$$
$$T_{\pm2}^{(2)} = I_\pm^2.$$

with

$$\begin{aligned} Q_0 &= Q_{zz}, \\ Q_{\pm1} &= Q_{zx} \pm iQ_{zy}, \\ Q_{\pm2} &= \tfrac{1}{2}(Q_{xx} - Q_{yy}) \pm iQ_{xy}. \end{aligned} \tag{2.27}$$

One can show (Appendix A) that the coefficients transform as $Q_m \mapsto e^{-im\zeta} Q_m$, under a rotation of angle ζ around the z-axis. Since the energy levels of the Hamiltonian only depends on the absolute quantities $|Q_m|$, the energy spectrum is invariant under rotations in the z axis: any two tensors related by a rotation in the xy plane produce identical NMR spectra for a fixed field orientation.

2.2. Spins coupled to a cavity

Spins coupled to a cavity text here.

Appendix

Rotation of the quadrupole tensor around the z-axis

A.

We start from the Cartesian, symmetric traceless tensor

$$Q = \begin{pmatrix} Q_{xx} & Q_{xy} & Q_{xz} \\ Q_{xy} & Q_{yy} & Q_{yz} \\ Q_{xz} & Q_{yz} & Q_{zz} \end{pmatrix}, \qquad \mathrm{Tr}\, Q = 0, \tag{A.1}$$

and rotate the axes by an angle ϕ about z with

$$R_z(\phi) = \begin{pmatrix} \cos\phi & \sin\phi & 0 \\ -\sin\phi & \cos\phi & 0 \\ 0 & 0 & 1 \end{pmatrix}. \tag{A.2}$$

Under this passive rotation,

$$Q' \;=\; R_z(\phi)\, Q\, R_z^{\top}(\phi). \tag{A.3}$$

Carrying out the multiplication gives

$$\begin{aligned} Q'_{xx} &= \cos^2\phi\, Q_{xx} + \sin^2\phi\, Q_{yy} + 2\sin\phi\cos\phi\, Q_{xy}, \\ Q'_{yy} &= \sin^2\phi\, Q_{xx} + \cos^2\phi\, Q_{yy} - 2\sin\phi\cos\phi\, Q_{xy}, \\ Q'_{xy} &= (\cos^2\phi - \sin^2\phi)\, Q_{xy} + \sin\phi\cos\phi\, (Q_{yy} - Q_{xx}), \\ Q'_{xz} &= \cos\phi\, Q_{xz} + \sin\phi\, Q_{yz}, \\ Q'_{yz} &= -\sin\phi\, Q_{xz} + \cos\phi\, Q_{yz}, \\ Q'_{zz} &= Q_{zz}. \end{aligned} \tag{A.4}$$

We define the spherical components (rank-2 irreducible combinations) as

$$\begin{aligned} Q_0 &= Q_{zz}, \\ Q_{\pm1} &= Q_{xz} \pm i Q_{yz}, \\ Q_{\pm2} &= \tfrac{1}{2}\,(Q_{xx} - Q_{yy}) \pm i\, Q_{xy}. \end{aligned} \tag{A.5}$$

Using A.4 in the definition of $Q'_{\pm1}$,

$$\begin{aligned} Q'_{+1} &= Q'_{xz} + i\, Q'_{yz} \\ &= \big(\cos\phi\, Q_{xz} + \sin\phi\, Q_{yz}\big) \;+\; i\big(-\sin\phi\, Q_{xz} + \cos\phi\, Q_{yz}\big) \\ &= (\cos\phi - i\sin\phi)\, Q_{xz} \;+\; (\sin\phi + i\cos\phi)\, Q_{yz} \;=\; e^{-i\phi}\, Q_{+1}. \end{aligned} \tag{A.6}$$

Similarly,

$$\begin{aligned} Q'_{-1} &= Q'_{xz} - i\, Q'_{yz} \\ &= \big(\cos\phi\, Q_{xz} + \sin\phi\, Q_{yz}\big) \;-\; i\big(-\sin\phi\, Q_{xz} + \cos\phi\, Q_{yz}\big) \\ &= (\cos\phi + i\sin\phi)\, Q_{xz} \;+\; (\sin\phi - i\cos\phi)\, Q_{yz} \\ &= e^{+i\phi}\,\big(Q_{xz} - iQ_{yz}\big) \;=\; e^{+i\phi}\, Q_{-1}. \end{aligned} \tag{A.7}$$

Let $\Delta \equiv Q_{xx} - Q_{yy}$. From (A.4),

$$\begin{aligned} Q'_{+2} &= \tfrac{1}{2}\,(Q'_{xx} - Q'_{yy}) + i\,Q'_{xy} \\ &= \tfrac{1}{2}\Big[\big(\cos^2\phi - \sin^2\phi\big)\Delta + 4\sin\phi\cos\phi\,Q_{xy}\Big] \\ &+ i\Big[\big(\cos^2\phi - \sin^2\phi\big)Q_{xy} - \sin\phi\cos\phi\,\Delta\Big]. \end{aligned} \tag{A.8}$$

Use the double-angle identities $\cos 2\phi = \cos^2\phi - \sin^2\phi$ and $\sin 2\phi = 2\sin\phi\cos\phi$ to rewrite

$$\begin{aligned} Q'_{+2} &= \tfrac{1}{2}\Big[\cos 2\phi\,\Delta + 2\sin 2\phi\,Q_{xy}\Big] + i\Big[\cos 2\phi\,Q_{xy} - \tfrac{1}{2}\sin 2\phi\,\Delta\Big] \\ &= \big(\tfrac{1}{2}\Delta + iQ_{xy}\big)\,\big(\cos 2\phi - i\sin 2\phi\big) \\ &= \big(\tfrac{1}{2}\Delta + iQ_{xy}\big)\,e^{-i2\phi} \;=\; e^{-i2\phi}\,Q_{+2}. \end{aligned} \tag{A.9}$$

By complex conjugation or repeating the steps with $-i$,

$$Q'_{-2} \;=\; e^{+i2\phi}\,Q_{-2}. \tag{A.10}$$

Since $Q'_{zz} = Q_{zz}$,

$$Q'_0 \;=\; Q_0. \tag{A.11}$$

Collecting the results,

$$Q'_m \;=\; e^{-im\phi}\,Q_m, \qquad m = 0, \pm 1, \pm 2. \tag{A.12}$$

Bibliography

Here are the references in citation order.

[1] Mitchel Weissbluth. *Atoms and Molecules*. Elsevier, Dec. 2, 2012. 730 pp. (cited on pages 2, 3).

[2] A. Abragam and B. Bleaney. *Electron Paramagnetic Resonance of Transition Ions*. Oxford Classic Texts in the Physical Sciences. Oxford: Oxford University Press, 2012. 911 pp. (cited on pages 2, 4, 8, 10).

[3] A. Senyshyn et al. 'Lattice Dynamics and Thermal Properties of CaWO4'. In: *Physical Review B* 70.21 (Dec. 23, 2004), p. 214306. DOI: 10.1103/PhysRevB.70.214306. (Visited on 10/16/2025) (cited on page 4).

[4] K. W. H. Stevens. 'Matrix Elements and Operator Equivalents Connected with the Magnetic Properties of Rare Earth Ions'. In: *Proceedings of the Physical Society. Section A* 65.3 (Mar. 1952), p. 209. DOI: 10.1088/0370-1298/65/3/308. (Visited on 09/01/2025) (cited on page 4).

[5] Bernal G. Enrique. 'Optical Spectrum and Magnetic Properties of Er3+ in CaWO4'. In: *The Journal of Chemical Physics* 55.5 (Sept. 1, 1971), pp. 2538–2549. DOI: 10.1063/1.1676445. (Visited on 09/01/2025) (cited on page 4).

[6] Edward H. Erath. 'Crystal Field Parameters for Erbium in Er (C2H5SO4)3·9H2O'. In: *The Journal of Chemical Physics* 34.6 (June 1, 1961), pp. 1985–1989. DOI: 10.1063/1.1731805. (Visited on 09/01/2025) (cited on page 4).

[7] S. A. Al'tshuler and Boris Michajlovič Kozyrev. *Electron Paramagnetic Resonance*. Burlington: Elsevier Science, 1964. 383 pp. (cited on page 4).

[8] HA Kramers. 'General Theory of Paramagnetic Rotation in Crystals'. In: *Proc. Acad. Sci. Amsterdam* 33 (1930), p. 959 (cited on page 4).

[9] Antipin, A.A. et al. 'Anisotropy of Er3+ Spin-Lattice Relaxation in LiYF4 Crystals'. In: *Soviet Journal of Experimental and Theoretical Physics* 23 (1981), pp. 2700–2707 (cited on page 6).

[10] J. M. Baker and Brebis Bleaney. 'Paramagnetic Resonance in Some Lanthanon Ethyl Sulphates'. In: *Proceedings of the Royal Society of London. Series A. Mathematical and Physical Sciences* 245.1241 (Jan. 1997), pp. 156–174. DOI: 10.1098/rspa.1958.0074. (Visited on 10/17/2025) (cited on page 6).

[11] H. M. Foley. 'Second-Order Magnetic Perturbations in Nuclear Quadrupole Spectra and the "Pseudo-Quadrupole" Effect in Diatomic Molecules'. In: *Physical Review* 72.6 (Sept. 15, 1947), pp. 504–505. DOI: 10.1103/PhysRev.72.504. (Visited on 09/01/2025) (cited on page 6).

[12] Frank S. Ham. 'Linear Effect of Applied Electric Field in Electron Spin Resonance'. In: *Physical Review Letters* 7.6 (Sept. 15, 1961), pp. 242–243. DOI: 10.1103/PhysRevLett.7.242. (Visited on 09/09/2025) (cited on page 6).

[13] A. Kiel and W. B. Mims. 'Electric-Field-Induced g Shifts for Loose Yb Ions in Three Scheelite Lattices'. In: *Physical Review B* 1.7 (Apr. 1, 1970), pp. 2935–2944. DOI: 10.1103/PhysRevB.1.2935. (Visited on 07/24/2025) (cited on page 6).

[14] W. B. Mims. 'Electric Field Shift in Paramagnetic Resonance for Four Ions in a Calcium Tungstate Lattice'. In: *Physical Review* 140 (2A Oct. 18, 1965), A531–A535. DOI: 10.1103/PhysRev.140.A531. (Visited on 07/24/2025) (cited on page 6).

[15] C. T. G. Knight et al. 'Solid-State Tungsten-183 Nuclear Magnetic Resonance Spectroscopy'. In: *Journal of the American Chemical Society* 108.23 (Nov. 1, 1986), pp. 7426–7427. DOI: 10.1021/ja00283a057. (Visited on 10/16/2025) (cited on page 7).

[16] Marianne Le Dantec et al. 'Twenty-Three–Millisecond Electron Spin Coherence of Erbium Ions in a Natural-Abundance Crystal'. In: *Science Advances* 7.51 (Dec. 15, 2021), eabj9786. DOI: 10.1126/sciadv.abj9786. (Visited on 10/17/2025) (cited on page 7).

[17] Andreas Erb and Jean-Côme Lanfranchi. 'Growth of High-Purity Scintillating CaWO4 Single Crystals for the Low-Temperature Direct Dark Matter Search Experiments CRESST-II and EURECA'. In: *CrystEngComm* 15.12 (Feb. 27, 2013), pp. 2301–2304. DOI: 10.1039/C2CE26554K. (Visited on 10/17/2025) (cited on page 7).

[18] Arthur Schweiger et al. *Principles of Pulse Electron Paramagnetic Resonance*. Oxford, New York: Oxford University Press, May 31, 2001. 604 pp. (cited on page 10).

[19] Charles P. Slichter. *Principles of Magnetic Resonance*. 3., enl. and updated ed., corr. 3. printing. Springer Series in Solid-State Sciences 1. Berlin Heidelberg: Springer, 1996. 655 pp. (cited on page 10).